Engineering Structures 118 (2016) 125–136

Contents lists available at ScienceDirect

Engineering Structures

journal homepage: www.elsevier.com/locate/engstruct

# A beam–column joint element for analysis of reinforced concrete frame structures

Peizhou Zhang [a,*], Shuang Hou [b], Jinping Ou [a,c]

[a] Faculty of Infrastructure Engineering, Dalian University of Technology, Dalian, China
[b] School of Civil & Transportation Engineering, South China University of Technology, Guangzhou, China
[c] School of Civil Engineering, Harbin Institute of Technology, Harbin, China

ARTICLE INFO

*Article history:*
Received 8 March 2014
Revised 9 March 2016
Accepted 10 March 2016

*Keywords:*
Beam–column joints
Reinforced concrete frames
Shear deformation
Low-ductility structures

ABSTRACT

Earthquake reconnaissance and laboratory tests reveal that the beam–column joints of existing RC frame structures in China are susceptible to failure, leading to severe structural damage. However, the inelastic response of joint elements is rarely considered in structural analysis or design. A new joint element considering shear deformation and bar-slip behaviour was proposed and verified using an extensive experimental data set. Two RC frame specimens with different details were modelled with the joint element and their simulated seismic responses were compared with experimental results in terms of global and local performance. Based on the simulation, the joint element proved to be reliable and suitable for 2D structural modelling. Finally, two reinforced concrete frame structures with the same dimensions and reinforcement ratios but different ductility are modelled with and without the proposed joint elements. The proposed joint element was shown to accurately predict the mechanical behaviour of such structures and their components, especially the hysteresis behaviour. Analysis shows that joint failure tends to happen in low-ductility structures and will reduce the ductility and the energy dissipation ability of the structure, even cause structural collapse. Compared with the new designed structures, seismic performance of the low-ductility ones is worse, with poor energy dissipation, weak collapse resistance and brittle failure modes.



## 1. Introduction

Earthquake reconnaissance and laboratory tests reveal that old beam–column joints of reinforced concrete (RC) frame structures built in China or other countries tend to suffer severe earthquake damage [1–5]. The typical failure modes include shear failure of joints and bond failure of the longitudinal beam in the joint panel, which may cause severe structural damage [6,7]. In order to consider the potential impact of joint failure on structural seismic response, researchers have developed various implicit explicit models of joint elements [8–15].

In the implicit ones the joint region is indirectly represented by nonlinear springs or plastic hinges in adjacent beams or columns. Such elements make it computationally efficient to determine the global influence of nonlinear joints on structural responses, but their shear deformation and bond-slip are hard to predict [16]. Explicit elements consider an explicit representation of the joint region and satisfy joint kinematics. They can easily be calibrated. The "BeamColumnJoint" element in OpenSees proposed by Lowes and Altoontash [12] in 2003 is one of elements widely used. The element was updated by Mitra and Lowes [13] in 2007 to make it easier to simulate the response of joints with a wide range of design parameters. However, there are still some limitations in its application. For example, it is difficult to consider complex cross sections of the adjacent beams and it is also difficult to account for different bond-slip relationships, such as behaviours of corroded reinforcing bars. Additionally, too many springs in this element may cause numerical convergence problems when applied in structural analysis, especially for the dynamic one, which is also described in Ghannoum's research [17].

A new beam–column joint element considering shear deformation and bar-slip behaviour is therefore proposed, and 16 interior joint specimens and two RC frame tests are presented to confirm its effectiveness and reliability at both the component and the structure level. The proposed joint element is applied to a study of the seismic performance of the low-ductility structures built before the 1990s in China.

* Corresponding author. Tel.: +86 17709816552.
*E-mail address:* zpz_87@163.com (P. Zhang).

http://dx.doi.org/10.1016/j.engstruct.2016.03.030
0141-0296/

## 2. The proposed beam–column joint element

### 2.1. Formulation

The Mitra–Lowes element comprises one shear panel component, eight bar-slip springs and four interface shear springs, as illustrated in Fig. 1. The shear panel simulates strength and stiffness loss due to failure of the joint panel; the bar-slip springs simulate strength and stiffness loss due to anchorage-zone damage; and the interface-shear springs simulate the shear transfer through friction at the beam or column ends. However, it is difficult for bar-slip springs to consider complex beam cross sections and account for different bond-slip behaviours in the joint panel. Moreover, too many bar-slip springs at the joint perimeter can easily cause numerical convergence problems in structural nonlinear analysis.

The joint element shown in Fig. 2 is proposed to overcome these limitations. It keeps the shear panel component but replaces the bar-slip springs by zero-length elements at the beam ends and it removes the bar-slip springs at the column ends for simplification. The constitutive model of reinforcing steel in a zero-length element can be defined by various stress–slip relations to introduce the additional angles $\Delta\theta_{bl}$ and $\Delta\theta_{br}$ at the beam ends accounting for different bond-slip behaviours, as described in Fig. 3. The additional angles calculated by section analysis are determined by the yield strength of the beam rebar $f_y$, the bond strengths $\tau_E$ and $\tau_Y$ for elastic and yielding steel, and beam rebar slip $s$. The shear forces $V_{br}$, $V_{bl}$, $V_{ct}$, $V_{cb}$, the axial forces $N_{br}$, $N_{bl}$, $N_{ct}$, $N_{cb}$, and the moments $M_{br}$, $M_{bl}$, $M_{ct}$, $M_{cb}$ at the joint perimeter are used to describe the force equilibrium. $\theta_{bl}$ and $\theta_{br}$ at the beam ends are the rotation angles associated with the moments $M_{bl}$ and $M_{br}$. $b$ and $h$ are the width and the height of the joint panel. The total moment $M_j$ and rotation angle $\theta_j$ for joint panel are defined by Eq. (1).

$$\theta_j = (u_{Vbr} + u_{Vbl})/b + (u_{Vct} + u_{Vcb})/h \tag{1a}$$

$$M_j = M_{ct} + M_{cb} - M_{bl} - M_{br} + (N_{ct}/2 - V_{br} - N_{cb}/2)\cdot b + (N_{bl}/2 + N_{ct} - N_{br}/2)\cdot h \tag{1b}$$

where $u_{Vbr}$, $u_{Vbl}$, $u_{Vct}$, $u_{Vcb}$ are the displacements associated with the shear forces $V_{br}$, $V_{bl}$, $V_{ct}$, $V_{cb}$ respectively, as shown in Fig. 3.

### 2.2. Shear panel response

Research has shown that the force-transfer mechanisms in a beam–column joint panel can be represented by diagonal compression strut, truss and confined mechanisms [18], as shown in Fig. 4. Modified compression field theory (MCFT) [19], diagonal compression strut model (DCSM) [13], and a simplified strut-and-tie model (STM) [20] can be used to represent them. Together they can be applied to predict the relationship of $M_j$ and $\theta_j$ for the rotational spring. Modified compression field theory is a general theory for the load–deformation behaviour of two-dimensional cracked RC structures subjected to shear. It was developed through testing of multiple RC panels subjected to uniform strain states. However, the uniform pure shear stress assumed by the theory is different from the complex stress state of a beam–column joint, so MCFT is not suitable for defining a joint's shear stress–strain relationship. Another approach is the diagonal compression strut model, in which a main strut is adopted to allow considering the diagonal compression strut and confined mechanisms without the truss mechanism.

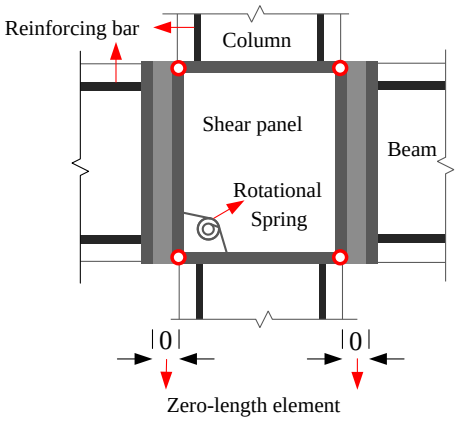


**Fig. 2.** Proposed joint element.

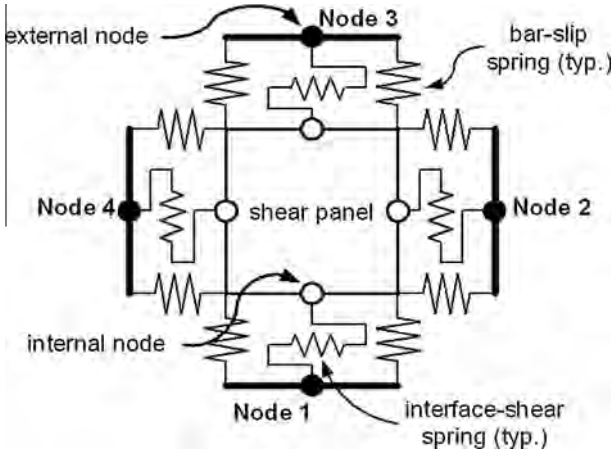


**Fig. 1.** Mitra–Lowes element (from Ref. [13]).

The simplified strut-tie model was developed to account for all these mechanisms by adding a sub-strut to simulate the shear effect of stirrups, as shown in Fig. 5. The truss mechanism is formed by the main strut, sub-strut and stirrup together. The STM was applied in this study to predict the joint's shear stress-rotation ($\tau_{j.STM}$, $\gamma_{j.STM}$) relationship. The Pinching4 material model [12] is recommended to describe any hysteresis, pinching, energy dissipation, and cyclic degradation of the joint's shear response. They are defined using a response envelope, an unload–reload path, and three damage rules that control how the joint's response path evolves, as shown in Fig. 6. This material model is particularly useful for simulating any pinched hysteresis of critical elements such as joints with low stirrup ratios.

The key points of the backbone curves ($M_{j.STM}$, $\theta_{j.STM}$) are defined by Eq. (2), which represents four damage states of the joint panels. State I is the crack opening state of concrete; state II is the strength yielding state of the stirrups; state III represents the joint shear stress reaching its maximum value; state IV means the shear failure of the joint region, as indicted in Fig. 6. The hysteresis rule is defined according to the approach of Mitra and Lowes [13].

$$\theta_{j.STM} = \gamma_{j.STM} \tag{2a}$$

$$M_{j.STM} = \tau_{j.STM}\cdot h_c \cdot h_b \cdot b_j \tag{2b}$$

where $h_c$ and $h_b$ are the width and the height of the joint; and $b_j$ is the maximum out-of-plane dimension of the beam or the column.

### 2.3. Bond-slip response

The most direct approach for defining bond-slip relations is to use the moment-rotation relationship to account for rotation caused by rebar slip [21]. Its properties can easily be determined.

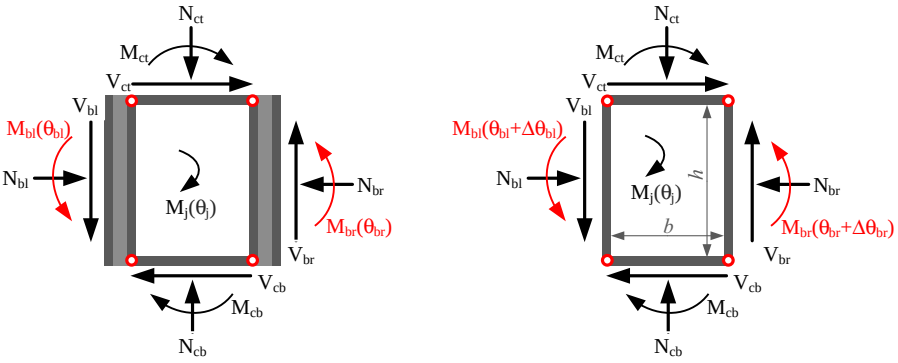


(a) Force equilibrium of the entire joint (b) Force equilibrium of the joint core

**Fig. 3.** Force equilibrium of the proposed joint element.

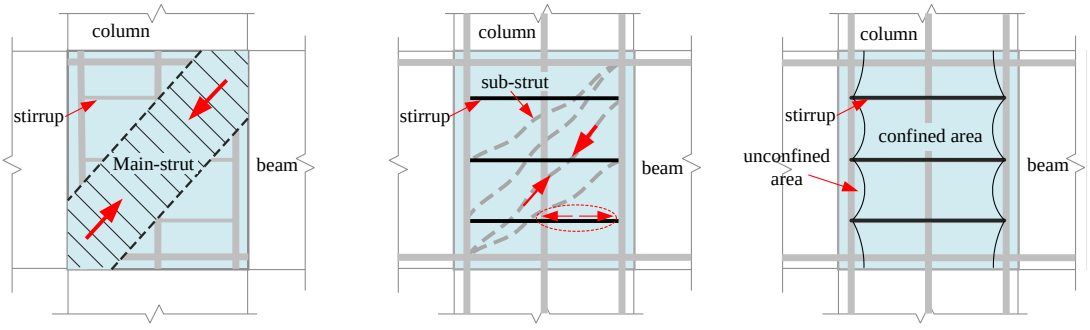


(a) Diagonal compression strut mechanism (b) Truss mechanism (c) Confined mechanism

**Fig. 4.** Force mechanisms of the beam–column joint panel.

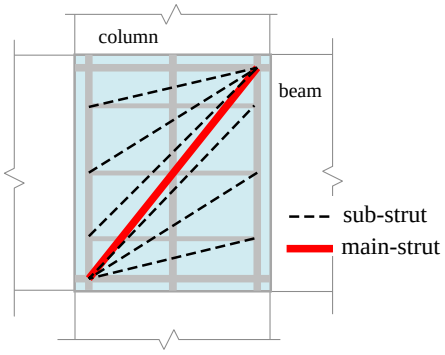


**Fig. 5.** Sketch of the STM's arrangement.

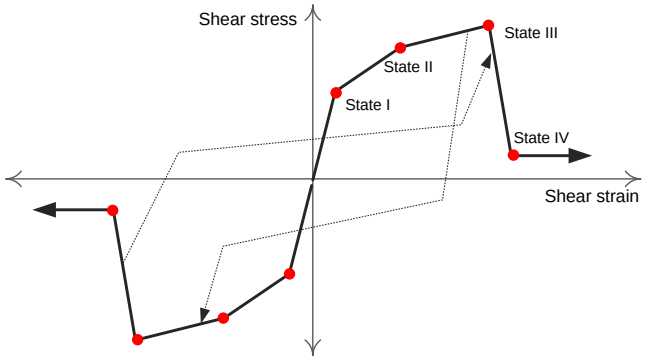


**Fig. 6.** A Pinching4 material model and four damage states of the joint region.

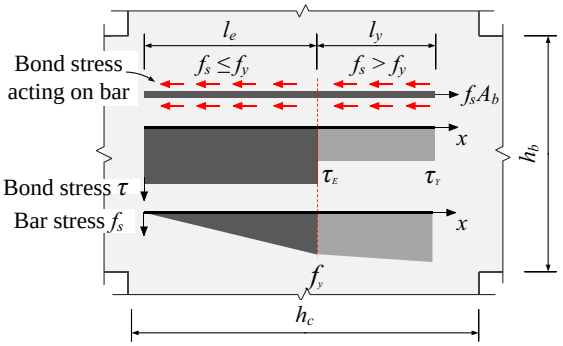


**Fig. 7.** Bond stress and bar stress distribution for a bar anchored in a beam–column joint.

In this study it was applied with a zero-length element to consider additional angles $\Delta\theta_{bl}$ and $\Delta\theta_{br}$ at the beam ends, as presented in Fig. 3(b). In a joint panel, an assumption of the mean bond stress and linear rebar stress distribution for an anchored bar loaded beyond yielding is applied to determine the beam and steel stress–slip relationship [12], as shown in Fig. 7. The parameters in Fig. 7 are defined as follows.

$$\text{For } f_s < f_y \quad s = \int_0^{l_{fs}} \tau_E \frac{\pi d_b}{A_b E} \cdot x dx = 2\frac{\tau_E l_{fs}^2}{E d_b} \tag{3a}$$

$$\text{For } f_s \geqslant f_y \quad s = \int_0^{l_e} \frac{4\tau_E}{d_b E} \cdot x dx + \int_{l_e}^{l_y+l_e} \left( \frac{f_y}{E} + \frac{4\tau_E}{d_b E_h}(x - l_e) \right) dx$$
$$= 2\frac{\tau_E l_e^2}{E d_b} + \frac{f_y}{E} l_y + \frac{2\tau_Y l_y^2}{E_h d_b} \tag{3b}$$

where

$$l_{f_s} = \frac{f_s}{\tau_{ET}} \cdot \frac{A_b}{\pi d_b}, \quad l_e = \frac{f_y}{\tau_{ET}} \cdot \frac{A_b}{\pi d_b}, \quad l_y = \frac{f_s - f_y}{\tau_{YT}} \cdot \frac{A_b}{\pi d_b}$$

where $E$ is the steel's elastic modulus; $E_h$ is the steel's hardening modulus assuming a bilinear stress–strain relationship; $\tau_{ET}$ and $\tau_{YT}$ are the mean bond strength for elastic and yielded steel respectively (as defined in Ref. [12]); $d_b$ and $A_b$ are the diameter and the area of the bar in the beam; and $l_e$ and $l_y$ are the lengths along the bar where the steel stress is smaller and larger than $f_y$, respectively. Based on these assumptions, the beam steel stress–slip relationship characterized by a monotonic envelope curve (as shown in Fig. 8) according to Eq. (3) can be used to replace the constitutive model of rebar in the zero-length element. In order to describe the pinching behaviour of bond slip, a Pinching4 material model (Fig. 12) is used to simulate the rebar's stress–slip behaviour, and the hysteresis parameters can be defined according to the approach of Lowes and Altoontash [12].

## 3. Evaluation of the joint components

### 3.1. Joint specimens

An experimental data set comprising 16 beam–column joint specimens with the same dimensions published by Fu [22] was selected to evaluate the proposed joint elements. The dimensions are shown in Fig. 9. Table 1 lists the reinforcement design details and Table 2 lists other design parameters defining the joint specimens. The design parameters shown in Table 2 are defined by Eqs. (4)–(9). The data set included 2D interior joint specimens with a wide range of structural parameters subjected to quasi-static cyclic loading in the laboratory.

(1) Measured concrete compressive strength, $f_c$ is the governing parameter of the joint shear behaviour [23].
(2) Observed joint shear strength defined by ACI-ASCE specification 352 [24]:

$$\tau_{\max\_ACI} = \frac{1}{h_c b_j} \left( \frac{M_L + M_R}{j h_b} - V_c \right) \tag{4}$$

where $V_c$ is the maximum column shear load; $M_L$ and $M_R$ are the moments at the beam-joint interface on the left and the right side respectively when the maximum column load is reached; $jh_b$ is the distance between the tension and compression resultants in the beam at the beam-joint interface.

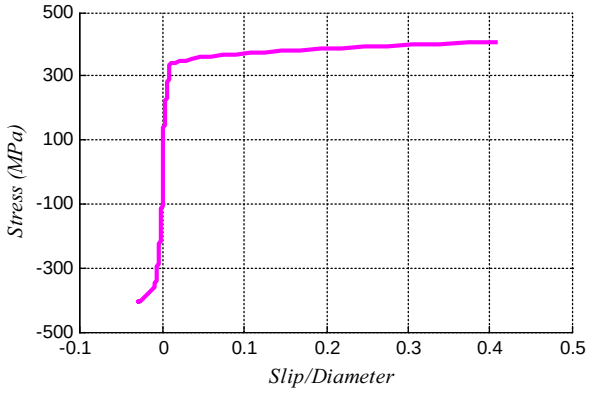


**Fig. 8.** A typical beam steel stress–slip relationship defined by Eq. (3).

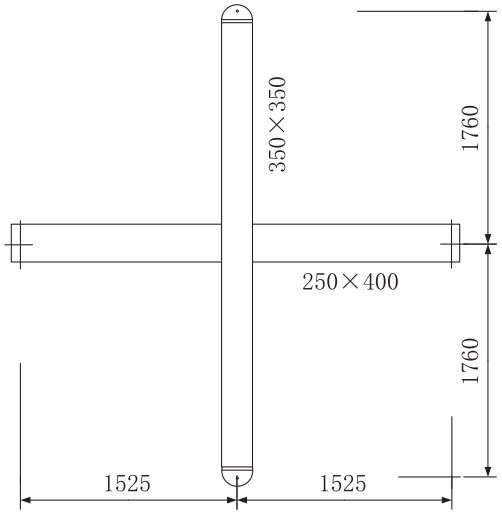


**Fig. 9.** Dimensions of the joint specimens.

(3) Bond index, $\mu$ is the average beam rebar bond stress in the joint [13]:

$$\mu = f_y d_b \Big/ \left( 2h_c \sqrt{f_c} \right) \tag{5}$$

(4) Joint horizontal transverse reinforcement ratio:

$$\rho_{sv} = A_{sv}/s_j b_j \tag{6}$$

where $A_{sv}$ is the area of a single layer of joint transverse reinforcement which passes through a plane normal to the beam axis; and $s_j$ is the spacing of joint transverse reinforcement layers.
(5) Column axial load ratio:

$$\gamma_N = N/(f_c A_c) \tag{7}$$

where $N$ is the column axial load; $A_c$ is the gross cross-sectional area of the column.
(6) Shear load ratio $\gamma_V$ is the ratio of average shear stress to concrete compressive strength, $f_c$ [25]:

$$\gamma_V = V_j/(f_c b_j h_c) \tag{8}$$

where $V_j$ is the shear force at the joint.
(7) The designed bending moment ratio $\gamma_M$ is the ratio of the designed bending moment of column $M_{uc}$ to the designed bending moment of beam $M_{ub}$ [22]:

$$\gamma_M = M_{uc}/M_{ub} \tag{9}$$

### 3.2. Simulation of the joint specimens

The proposed joint element was used to simulate the joint specimens using OpenSees software, and the simulation results were compared with the test results. Fig. 10 shows one of the typical numerical models of the joint specimens which was subjected to lateral loading under displacement control at the beam ends. Meanwhile, constant axial loading was maintained on the column. The nonlinear response of the beams and columns was simulated using the force-based element, and the Concrete01 and Steel02 models were used for the concrete and rebar respectively. The joint element in Fig. 2 was used to simulate joint element, as shown in Fig. 10.

**Table 1**
Reinforcement design for joint specimens.

| Joint specimens | Upper beam section | | Lower beam section | | Stirrups at beam ends | | Rebars in one side of column | | Stirrups at column ends | | Rebars in one side of joint panel | |
|---|---|---|---|---|---|---|---|---|---|---|---|---|
| | (mm) | $f_y$ (MPa) | (mm) | $f_y$ (MPa) | (mm) | $f_y$ (MPa) | (mm) | $f_y$ (MPa) | (mm) | $f_y$ (MPa) | (mm) | $f_y$ (MPa) |
| J-1 | 3Φ18 | 397 | 3Φ18 | 397 | Φ8@100 | 298 | 4Φ22 | 363 | Φ8@100 | 298 | – | – |
| J-2 | 3Φ18 | 397 | 3Φ18 | 397 | Φ8@100 | 298 | 4Φ22 | 363 | Φ8@100 | 298 | – | – |
| J-3 | 3Φ16 | 388 | 3Φ16 | 388 | Φ8@100 | 298 | 3Φ22 | 363 | Φ8@100 | 298 | – | – |
| J-4 | 3Φ16 | 388 | 3Φ16 | 388 | Φ8@100 | 298 | 3Φ22 | 363 | Φ8@100 | 298 | – | – |
| J-5 | 3Φ18 | 397 | 3Φ18 | 397 | Φ8@100 | 298 | 4Φ22 | 363 | Φ8@100 | 298 | – | – |
| | 1Φ16 | 388 | 1Φ16 | 388 | | | | | | | | |
| J-6 | 3Φ18 | 397 | 3Φ18 | 397 | Φ8@100 | 298 | 4Φ22 | 363 | Φ8@100 | 298 | – | – |
| | 1Φ16 | 388 | 1Φ16 | 388 | | | | | | | | |
| J-7 | 5Φ18 | 376 | 3Φ18 | 376 | Φ8@100 | 359 | 4Φ20 | 350 | Φ8@100 | 359 | 1Φ14 | 365 |
| J-8 | 3Φ18 | 376 | 3Φ18 | 376 | Φ8@100 | 359 | 3Φ16 | 423 | Φ8@100 | 359 | 1Φ14 | 365 |
| J-9 | 4Φ18 | 376 | 2Φ18 | 376 | Φ8@100 | 359 | 3Φ20 | 350 | Φ8@100 | 359 | 1Φ14 | 365 |
| J-10 | 4Φ18 | 376 | 2Φ18 | 376 | Φ8@100 | 359 | 3Φ16 | 423 | Φ8@100 | 359 | 1Φ14 | 365 |
| J-11 | 5Φ18 | 400 | 3Φ16 | 375 | Φ8@100 | 390 | 5Φ16 | 375 | Φ8@100 | 390 | – | – |
| J-12 | 5Φ18 | 400 | 3Φ16 | 375 | Φ8@100 | 390 | 3Φ14 | 380 | Φ8@100 | 390 | – | – |
| J-13 | 4Φ18 | 400 | 2Φ16 | 375 | Φ8@100 | 390 | 4Φ18 | 400 | Φ8@100 | 390 | 1Φ14 | 380 |
| | 2Φ16 | 375 | 2Φ18 | 400 | | | | | | | | |
| J-14 | 4Φ18 | 400 | 2Φ16 | 375 | Φ8@100 | 390 | 5Φ14 | 375 | Φ8@100 | 390 | 1Φ14 | 380 |
| | 2Φ16 | 375 | 2Φ18 | 400 | | | | | | | | |
| J-15 | 6Φ18 | 400 | 4Φ18 | 400 | Φ8@100 | 390 | 5Φ18 | 400 | Φ8@100 | 390 | 1Φ14 | 380 |
| J-16 | 6Φ18 | 400 | 4Φ18 | 400 | Φ8@100 | 390 | 4Φ14 | 375 | Φ8@100 | 390 | 1Φ14 | 380 |

**Table 2**
Design details of the joint specimens.

| Joint specimens | $f_c$ (Mpa) | $\tau_{max\_ACI}$ (Mpa) | $h_c/d_b$ | | $\mu$ | | $\rho_{sv}$ | $\gamma_N = N/f_cA$ | $\gamma_V = V_j/f_cb_jh_c$ | $\gamma_M = M_{uc}/M_{ub}$ |
|---|---|---|---|---|---|---|---|---|---|---|
| | | | Top | *Bot* | Top | *Bot* | | | | |
| J-1 | 46.0 | 5.07 | 19.44 | 19.44 | 1.73 | 1.73 | 0.01 | 0.05 | 0.125 | 2.51 |
| J-2 | 38.5 | 5.43 | 19.44 | 19.44 | 1.89 | 1.89 | 0.01 | 0.36 | 0.161 | 2.80 |
| J-3 | 34.2 | 4.88 | 21.88 | 21.88 | 1.74 | 1.74 | 0.01 | 0.05 | 0.130 | 2.44 |
| J-4 | 36.7 | 4.88 | 21.88 | 21.88 | 1.68 | 1.68 | 0.01 | 0.36 | 0.113 | 2.44 |
| J-5 | 44.2 | 6.63 | 19.44 | 19.44 | 1.76 | 1.76 | 0.01 | 0.05 | 0.165 | 1.96 |
| J-6 | 30.6 | 6.35 | 19.44 | 19.44 | 2.12 | 2.12 | 0.01 | 0.36 | 0.238 | 2.13 |
| J-7 | 36.9 | 5.75 | 19.44 | 19.44 | 1.83 | 1.83 | 0.02 | 0.05 | 0.197 | 1.57 |
| J-8 | 33.6 | 5.51 | 19.44 | 19.44 | 1.91 | 1.91 | 0.02 | 0.25 | 0.217 | 1.35 |
| J-9 | 35.0 | 5.07 | 19.44 | 19.44 | 1.87 | 1.87 | 0.01 | 0.05 | 0.156 | 1.73 |
| J-10 | 29.3 | 4.52 | 19.44 | 19.44 | 2.05 | 2.05 | 0.01 | 0.25 | 0.186 | 1.52 |
| J-11 | 31.5 | 5.91 | 19.44 | 21.88 | 1.98 | 1.76 | 0.02 | 0.10 | 0.230 | 1.24 |
| J-12 | 29.3 | 5.91 | 19.44 | 21.88 | 2.18 | 1.94 | 0.01 | 0.25 | 0.238 | 1.12 |
| J-13 | 34.7 | 6.80 | 20.23 | 20.59 | 1.93 | 1.89 | 0.02 | 0.15 | 0.267 | 1.22 |
| J-14 | 33.3 | 6.80 | 20.23 | 20.59 | 1.97 | 1.93 | 0.02 | 0.25 | 0.256 | 1.22 |
| J-15 | 29.6 | 6.93 | 19.44 | 19.44 | 2.17 | 2.17 | 0.02 | 0.15 | 0.310 | 1.25 |
| J-16 | 30.7 | 6.29 | 19.44 | 19.44 | 2.13 | 2.13 | 0.02 | 0.45 | 0.310 | 1.07 |
| Maximum | 46.00 | 6.93 | 21.88 | 21.88 | 2.18 | 2.17 | 0.02 | 0.45 | 0.310 | 2.80 |
| Minimum | 29.30 | 4.52 | 19.44 | 19.44 | 1.68 | 1.68 | 0.01 | 0.05 | 0.113 | 1.07 |
| Mean | 34.63 | 5.80 | 19.85 | 20.20 | 1.93 | 1.90 | 0.01 | 0.20 | 0.206 | 1.72 |

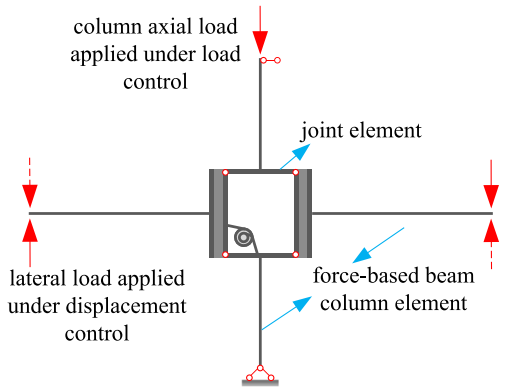


**Fig. 10.** Joint specimen modelling.

### 3.3. Simulated and experimental results

Simulated and experimental results are compared in Table 3. Related work has shown that the failure mode sequence has great influence on the joint shear behaviour [23], so three main failure mechanisms are considered in the present study (only two types were recorded in the experiment): bond-slip failure of the beam reinforcing bars without joint failure (SF), beam flexural yielding followed by joint failure (BYJF) and beam flexural yielding followed by bond-slip failure (BYSF). Bond-slip failure might occur at slip greater than 3 mm [12]; beam yielding will occur if bar stress is greater than its yield strength; joint failure would happen when its damage state exceeds the State II, as shown in Fig. 6. The response parameters in Table 3 are defined and explained as follows:

(1) Failure modes. Overall, the proposed element simulates the correct inelastic failure mechanism with good accuracy for specimens exhibiting SF(3/3) and moderate accuracy for

**Table 3**
Comparison of simulated and experimental results.

| Joint specimens | Failure modes | | Initial stiffness (kN/mm) | | Post yield stiffness (kN/mm) | | Reloading stiffness (kN/mm) | | Unloading stiffness (kN/mm) | | Pinching ratio | | Max. Col load (kN) | | Drift at max. Load (mm) | |
|---|---|---|---|---|---|---|---|---|---|---|---|---|---|---|---|---|
| | Sim | Test | Sim | Test | Sim | Test | Sim | Test | Sim | Test | Sim | Test | Sim | Test | Sim | Test |
| J-1 | SF | SF | 7.5 | 7.9 | 0.5 | 0.9 | 2.2 | 2.3 | 7.3 | 7.0 | 0.2 | 0.1 | 103.0 | 91.6 | 67.4 | 31.7 |
| J-2 | SF | SF | 9.3 | 9.9 | 0.5 | 0.5 | 1.4 | 1.8 | 9.1 | 9.0 | 0.3 | 0.2 | 105.0 | 92.3 | 61.8 | 45.9 |
| J-3 | SF | SF | 5.9 | 8.7 | 0.4 | 0.7 | 1.2 | 1.4 | 6.3 | 6.9 | 0.3 | 0.2 | 74.6 | 97.7 | 39.8 | 37.7 |
| J-4 | BYSF | BYJF | – | – | – | – | – | – | – | – | – | – | – | – | – | – |
| J-5 | BYJF | BYJF | 8.7 | 9.0 | 0.7 | 0.5 | 2.0 | 2.5 | 8.6 | 13.6 | 0.2 | 0.1 | 119.1 | 117.3 | 38.9 | 42.9 |
| J-6 | BYSF | BYJF | 8.4 | 14.2 | 0.9 | 0.4 | 3.2 | 3.2 | 9.1 | 6.1 | 0.2 | 0.1 | 118.0 | 122.7 | 41.6 | 26.8 |
| J-7 | BYJF | BYJF | 8.0 | 5.3 | 0.8 | 0.7 | 6.4 | 5.3 | 6.8 | 6.8 | 0.1 | 0.1 | 141.5 | 123.3 | 40.2 | 42.2 |
| J-8 | BYJF | BYJF | 7.8 | 6.0 | 0.6 | 0.7 | 0.9 | 2.1 | 6.0 | 6.1 | 0.1 | 0.1 | 140.9 | 119.2 | 59.7 | 66.9 |
| J-9 | BYJF | BYJF | 7.7 | 7.6 | 0.5 | 0.4 | 3.6 | 6.0 | 8.0 | 8.2 | 0.2 | 0.1 | 113.7 | 115.9 | 59.1 | 31.9 |
| J-10 | BYJF | BYJF | 7.0 | 10.9 | 0.3 | 0.1 | 1.2 | 2.3 | 7.9 | 7.6 | 0.2 | 0.2 | 110.8 | 101.8 | 60.8 | 44.5 |
| J-11 | BYJF | BYJF | – | – | – | – | – | – | – | – | – | – | – | – | – | – |
| J-12 | BY* | BYJF | 8.6 | 6.0 | 0.6 | 1.9 | 1.7 | 2.3 | 6.2 | 4.8 | 0.1 | 0.1 | 128.1 | 133.8 | 40.9 | 27.0 |
| J-13 | BYJF | BYJF | 7.9 | 9.8 | 0.5 | 0.8 | 2.2 | 2.5 | 8.0 | 7.4 | 0.2 | 0.1 | 125.3 | 137.1 | 59.5 | 33.5 |
| J-14 | BYJF | BYJF | – | – | – | – | – | – | – | – | – | – | – | – | – | – |
| J-15 | BYJF | BYJF | 7.8 | 9.0 | 0.9 | 0.8 | 3.0 | 6.9 | 7.7 | 7.8 | 0.1 | 0.1 | 140.7 | 142.3 | 59.6 | 30.6 |
| J-16 | BY* | BYJF | 9.2 | 10.0 | 0.5 | 0.8 | 2.7 | 2.5 | 5.4 | 8.0 | 0.5 | 0.1 | 127.0 | 135.5 | 38.5 | 34.6 |
| Mean of sim/test | – | – | 0.97 | | 1.15 | | 0.79 | | 1.01 | | 2.00 | | 1.02 | | 1.42 | |
| COV of sim/test | – | – | 0.08 | | 0.51 | | 0.06 | | 0.05 | | 1.58 | | 0.01 | | 0.16 | |

(1) There are no experimental results for J-4, J-11 and J-14; (2) * Means column flexural failure occur at last.

BYJF(9/13). Due to the small designed bending moment ratios for specimens J-12 and J-16, column flexural failures occur unexpectedly at last in the analytical models.

(2) Initial and unloading stiffness. The initial and unloading stiffness obtained through numerical simulation agreed well with experimental results. The average ratios of the simulated stiffness to the experimental stiffness were 0.97 and 1.01 with coefficients of variation (COV) of 8% and 5%. Unloading stiffness is a measure of stiffness deterioration exhibited by the shear-panel and/or the bar-slip component when the global system reaches maximum load.

(3) Post yield and reloading stiffness. The proposed joint element did not predict post-yield or reloading stiffness. The average ratios of the simulated stiffness to the experimental stiffness were 1.15(51%) and 0.79(6%). For this simulation, the post yield stiffness was affected by the flexural stiffness of the beams and columns, by the degraded post-peak response of the sheared panel, and by the hardening response of the bar-slip components.

(4) Maximum column load. The joint element was able to represent correctly the behaviour of the sub-assembly in the tests, with the average ratio of simulation to test results of 1.02. The COV of 1% was considered good.

(5) Drift at maximum column load. The joint element did not predict the drift at maximum strength well. For all of the specimens, the average ratio of simulated to test drift was 1.42 with a COV of 16%.

(6) Pinching ratio is defined as the ratio of the column load without drift to the maximum load using data from the cycle. On average, the joint element predicted the pinching ratio poorly with a mean value of 2.0 and a COV of 158%.

Clearly the predictive accuracy the proposed joint element varied greatly for different responses, at least with this software package. The accuracy was high for initial stiffness, unloading stiffness and maximum column load, moderate for reloading stiffness, post yield stiffness, failure mode and pinching ratio. Specimens, J-1, J-2, J-3, J-5, J-6, J-8 all showed symmetrical force–displacement responses and the typical simulated results of proposed element and Mitra–Lowes element are compared in Fig. 11(a). It can be seen that the prediction by the proposed joint element on the stiffness, maximum strength, pinching region and peak points can be much better than that by the existing element. Considering the unsymmetrical reinforcements, specimens J-7, J-9, J-10, J-12, J-13, J-15, J-16 showed unsymmetrical global responses and the analytical results of J-12 are plotted in Fig. 11(b). Due to the small designed bending moment ratio, column flexural failures occur unexpectedly in both analytical models and the proposed joint element seems more reasonable to predict the pinching region and softening point. On the negative side, the softening branch is caused by joint failure in the experiment, but they all overestimate the strength of the beam–column connection.

## 4. Evaluation of the joint elements on the structural level

The proposed joint element was applied to predicting the joint shear response and the bond slip of the beam and rebar in the structural model presented in Fig. 12. The implementation procedure with the OpenSees software was as follows. A displacement-based element [26] with 4 integration points was applied to simulate the behaviour of the beams and columns. The Steel02 and Concrete01 material models [26] were used to simulate the behaviour of the rebar and the unconfined concrete respectively, and ConfinedConcrete01 [27] was used for the core concrete. The Pinching4 subroutine was used to simulate the behaviour of the rotational spring in the joint panel and bond-slip response at the beam ends. The effects of rebar buckling and bond slip between reinforcing bar and concrete in beams and columns as well as of strain penetration in the base anchorage blocks are not considered in this study.

To evaluate this element on the structural level, two RC frame tests, without a slab (RC frame I) and with a slab (RC frame II) were modelled with (wJoint) and without (woJoint) joint elements. The simulated and experimental results were compared in terms of global and local performance to verify the reliability and effectiveness of the proposed joint element. The geometries and design details of the two RC frames are shown in Fig. 13, and the properties of their structural material are listed in Tables 4 and 5.

### 4.1. RC frame I

RC frame I, a two-bay, three-storey and 1/2.0 scaled frame, was designed in compliance with China's code 78 [28] of 1986. The

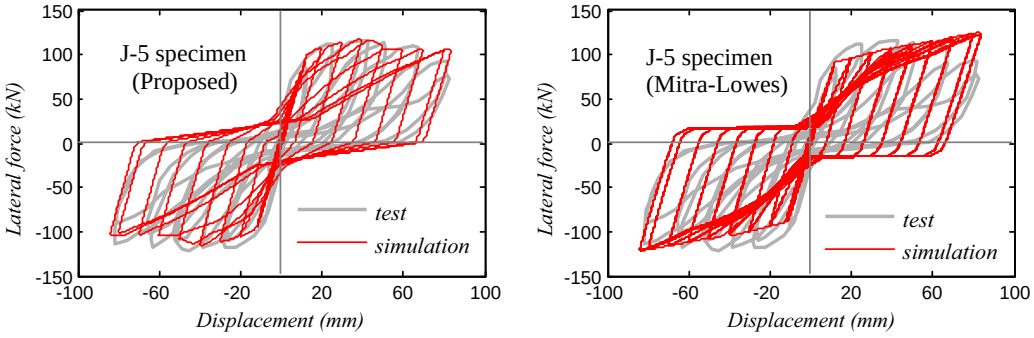


(a) A typical simulated result for the symmetrical force-displacement responses

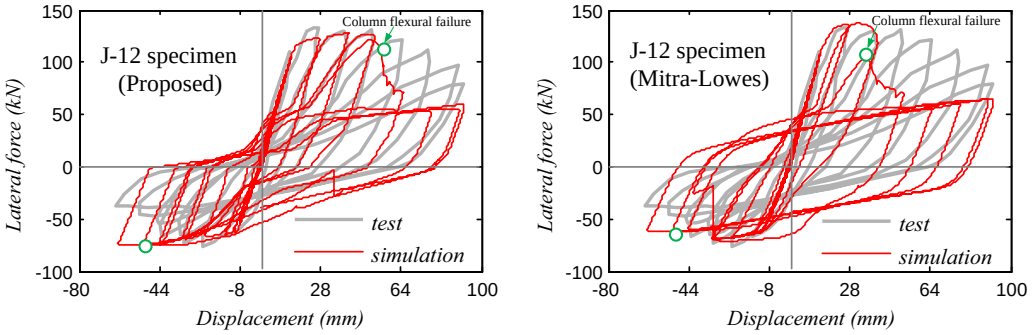


(b) A typical simulated result for the unsymmetrical force-displacement responses

**Fig. 11.** Typical simulated results for joint specimens.

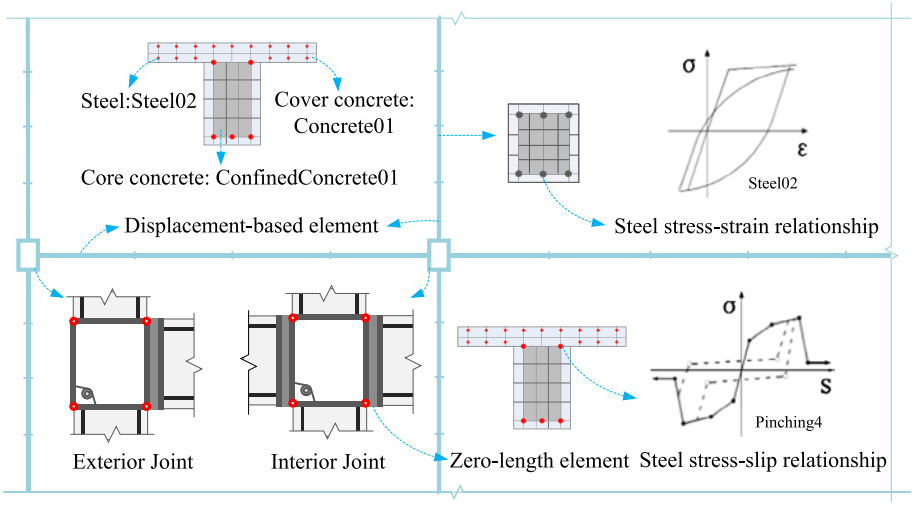


**Fig. 12.** Structural modelling details with the proposed joint element.

geometry and details were selected to be representative of elements used in many existing seven-storey RC frame buildings in China [29]. The design details were as follows: the beam rebar ratio was 0.5–1.06%; column rebar ratio was 0.36–0.64%; $\gamma_V$ of all joints was 0.86%; the $\gamma_N$ of the interior and exterior columns was 0.34 and 0.2 respectively. The frame was subjected to quasi-static cyclic loading at point A under load control before frame yielding, followed by displacement control after yielding. The design details of the frame tested are presented in Fig. 13(a).

woJoint and wJoint structural models were evaluated. Their first-order periods were 0.083 s, close to the experimental result of 0.09 s. Fig. 14 shows the base shear verse top displacement curves for RC frame I with and without joint elements. Comparing the results of two models shows that the simulated result with the wJoint model was almost identical to the test result, including the backbone curve, reloading, unloading, and the pinching ratio. The result with the woJoint model shows some discrepancy with the test results. Shear failure did not occur in all the beam–column joints, but the slippage of beam and rebar was very large, about 10 mm at its peak.

### 4.2. RC frame II

A series of quasi-static tests of RC frame structures was carried out at Tsinghua University to investigate the seismic damage mechanism observed after the Wenchuan earthquake. The tests

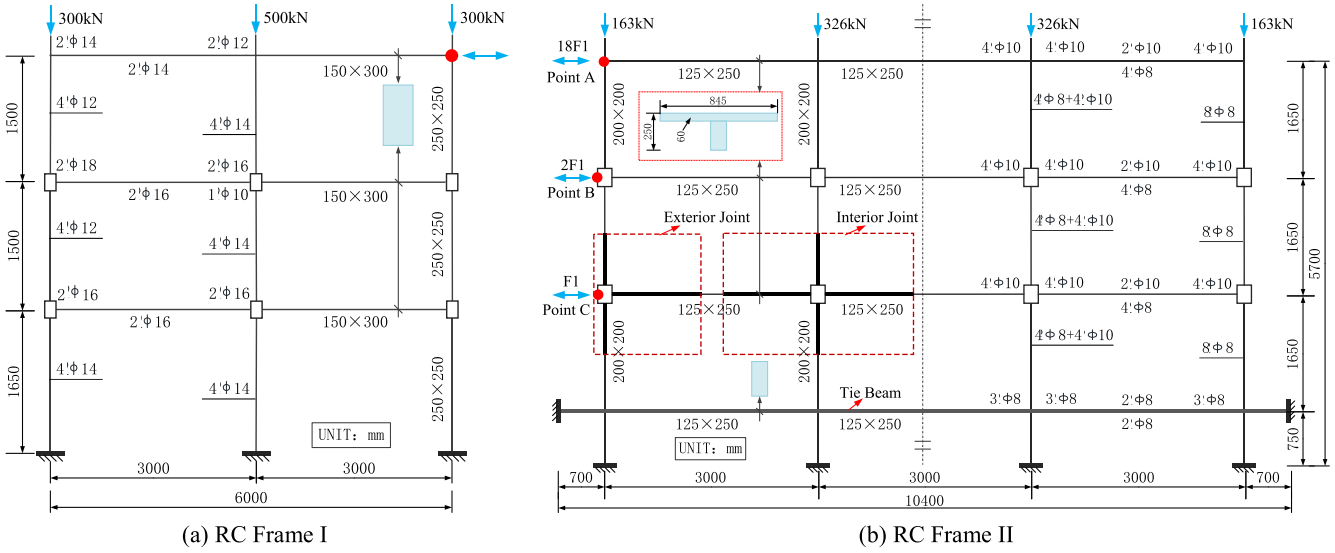


(a) RC Frame I (b) RC Frame II

**Fig. 13.** Geometries and details of the RC frame tests.

**Table 4**
Properties of the structural material: (a) design parameters of the concrete.

| RC frames | Location of beams and columns | $f_{cu,150mm}$ (MPa) | $f_c$ (MPa) | $E_c$ (MPa) |
|---|---|---|---|---|
| RC frame I | Beams and columns for the whole structure | – | 40.0 | 2.55e4 |
| RC frame II | Beams at the base floor | 36.8 | 28.0 | 2.80e4 |
| | Tie beams and columns | 31.8 | 24.2 | 2.42e4 |
| | Beams and columns on the 1st floor | 36.2 | 27.5 | 2.75e4 |
| | Beams and columns on the 2nd floor | 34.7 | 26.4 | 2.64e4 |
| | Beams and columns on the 3rd floor | 33.6 | 25.5 | 2.55e4 |

**Table 5**
Properties of the structural material: (b) design parameters of the reinforcing bars.

| RC frames | Rebar | $d$ (mm) | $f_y$ (MPa) | $f_u$ (MPa) | $\varepsilon_y$ | $E_s$ (MPa) | Elongation (%) |
|---|---|---|---|---|---|---|---|
| RC frame I | Φ18 | 18.0 | 388.4 | 588.1 | 2.13e−3 | 1.82e5 | – |
| | Φ16 | 16.0 | 413.9 | 618.2 | 2.46e−3 | 1.68e5 | – |
| | Φ14 | 14.0 | 378.9 | 614.3 | 2.03e−3 | 1.87e5 | – |
| | Φ12 | 12.0 | 400.1 | 576.2 | 2.02e−3 | 1.98e5 | – |
| | Φ10 | 10.0 | 428.0 | 585.7 | 2.47e−3 | 1.73e5 | – |
| RC frame II | Φ10 | 10.0 | 481.0 | 745.0 | 2.00e−3 | 2.65e5 | 23.6 |
| | Φ8 | 8.0 | 582.0 | 855.0 | 2.00e−3 | 2.90e5 | 28.8 |
| | Φ6 | 6.0 | 441.0 | 529.0 | 2.20e−3 | 2.04e5 | 34.2 |
| | Φ4 | 4.0 | 390.0 | 414.0 | 2.10e−3 | 1.95e5 | 26.7 |

included a frame, two beam–column joints and four columns [30]. Their three-bay, three-storey, and 1/2 scaled RC frame results were used to verify the effectiveness of the method in analysing RC frames with slabs, as shown in Fig. 13(b). That frame was designed in compliance with China's code 2001 [25]. Axial loads (163 kN and 326 kN) were applied on the top exterior and top interior columns; lateral loads were applied to points A, B, and C (Fig. 13) in a ratio of 18:2:1 under load control first and then displacement control. The geometries and details are presented in Fig. 13(b), and the properties of the structural material are listed in Tables 4 and 5.

The dashed line in Fig. 15(a) represents the simulated load–displacement hysteresis curve, which is the result of the model without joint elements. The backbone curves of the simulation and the test are close, but the hysteresis performance differs in the terms of the reloading stiffness, the unloading stiffness and the energy consumption. The test results show that cracks occurred in the exterior joint (at the tie-beam floor) and interior joint (at the first floor) at the 5th load cycle. The maximum storey drift of the frame reached 2% at the 12th load cycle, and the first floor joints showed significant damage and large shear deformation (Fig. 16). The failure of the concrete in the joint core became very serious from the 17th to 20th load cycles. The test results show that the first floor joints suffered serious damage, but damage to joints at the second floor level was slight. Based on this analysis, it can be concluded that good hysteretic performance of the woJoint model might have been caused by the lack of joint modelling.

So the results with RC frame II suggest conclusions similar to those with frame I. Compared with the woJoint model, the

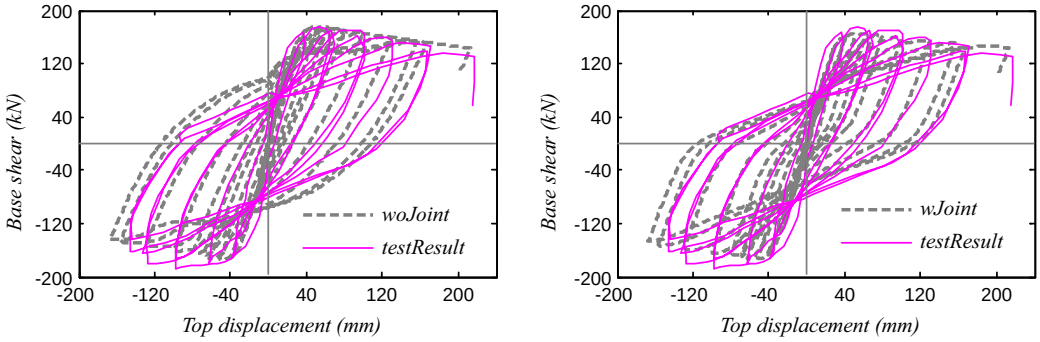


(a) Model without joint elements (b) Model with joint elements

**Fig. 14.** Hysteresis curves of the RC frame I with and without joint elements.

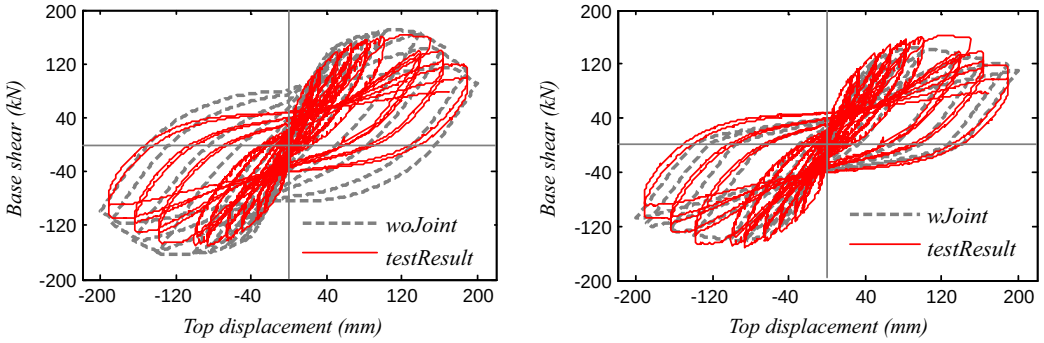


(a) Result of the model without joint elements (b) Result of the model with joint elements

**Fig. 15.** Hysteresis curves of RC frame II.

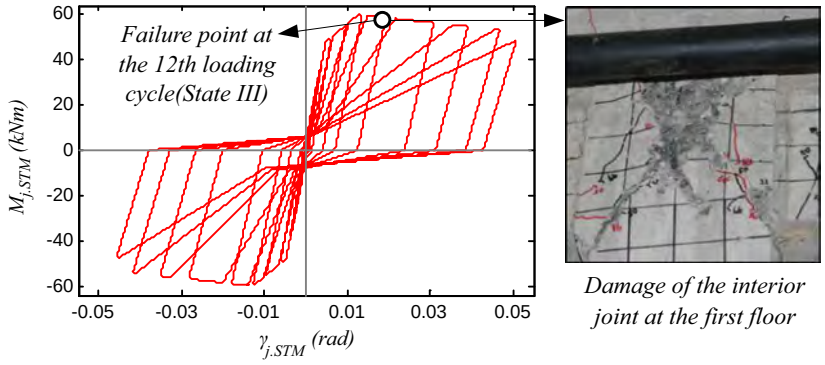


**Fig. 16.** Simulated moment-shear strain response ($M_{j.STM}$, $\gamma_{j.STM}$) and experimental damage to the joint at the first floor.

load–displacement curve of the wJoint model was much closer to the test results in reloading, unloading and pinching. At the local level, Fig. 16 shows the moment-shear strain response of the interior joint at the first floor and the corresponding damage to that joint panel at the 12th load cycle. The damage state agrees well with the simulated result.

The structural modelling method with the proposed joint elements can therefore be trusted to assess the seismic performance of RC frame structures.

## 5. Application of the joint element to low-ductility RC structures

### 5.1. Details of the RC structures

Two RC frame structures with the same dimensions and reinforcement ratios but different ductility [31] were selected to assess the seismic performance of low-ductility structures. The difference between them is shown in Table 6. The low-ductility specimen was

**Table 6**
Design parameters of the two RC frame structures.

| Structural types | Grade of concrete | $\gamma_N$ | Diameter of stirrups (mm) | Spacing of stirrups (mm) | Type of stirrups |
|---|---|---|---|---|---|
| Low-ductility RC frame | C20 | 0.2 | 6 | 200 | S1 |
| Newer RC frame | C30 | 0.2 | 8 | 100 | S2 |

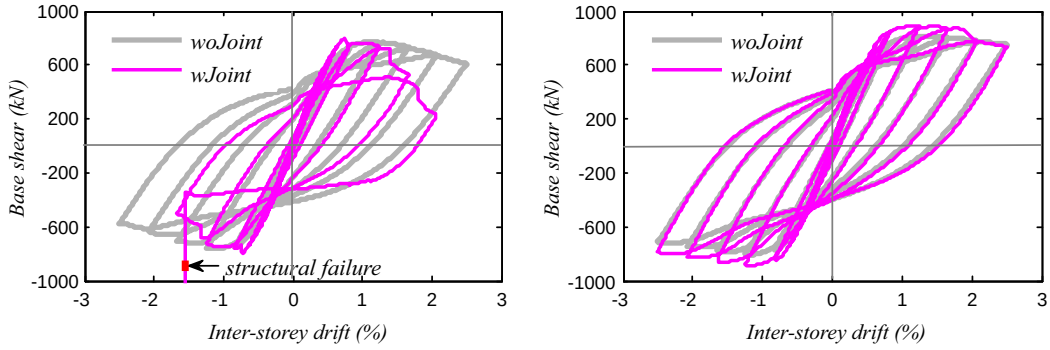


(a) Low-ductility RC frame structure (b) Newer RC frame structure

**Fig. 17.** Mechanical performance of the two structures under cyclic loading.

designed in compliance with code 78, and thus represents the typical existing RC frame building built before the 1990s in China. Newer ones were designed in compliance with code 2001 after 1990.

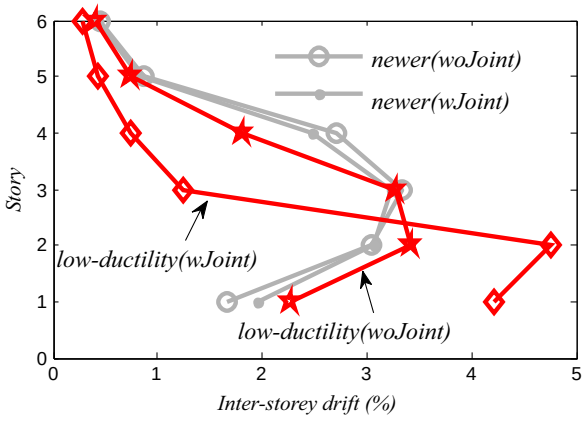


**Fig. 18.** Distribution of the maximum inter-storey drifts.

(1) Stirrups and longitudinal reinforcing bars are grades HPB235 and HRB335; the mean of their yield strengths are 272 MPa and 388 MPa; their elastic modulus are 210 GPa and 200 GPa.
(2) The concrete is grade C20 or C30; the means of their compressive strengths, $f_c$ are 17.5 Mpa and 26.1 MPa; their elastic modulus are 28.3 GPa and 32.36 GPa.
(3) The types of stirrups in table are described in Ref. [31].

### 5.2. Quasi-static analysis with/without joint elements

Quasi-static cyclic analysis with an inverted triangle load pattern was applied to study the mechanical performance of the two structures at 2% of the total height (480 mm). The maximum storey drift of the structural collapse state was adopted as the target displacement according to code 2001. The result for the new designed structure was very close regardless of whether or not the proposed joint element was incorporated, but for the low-ductility design the joint element caused the analytical results to differ greatly, as is shown in Fig. 17(a). The wJoint model predicted the failure mode of the low-ductility structure well, which shows that if joint elements aren't considered in simulating low-ductility frames, the failure modes of structures may not be

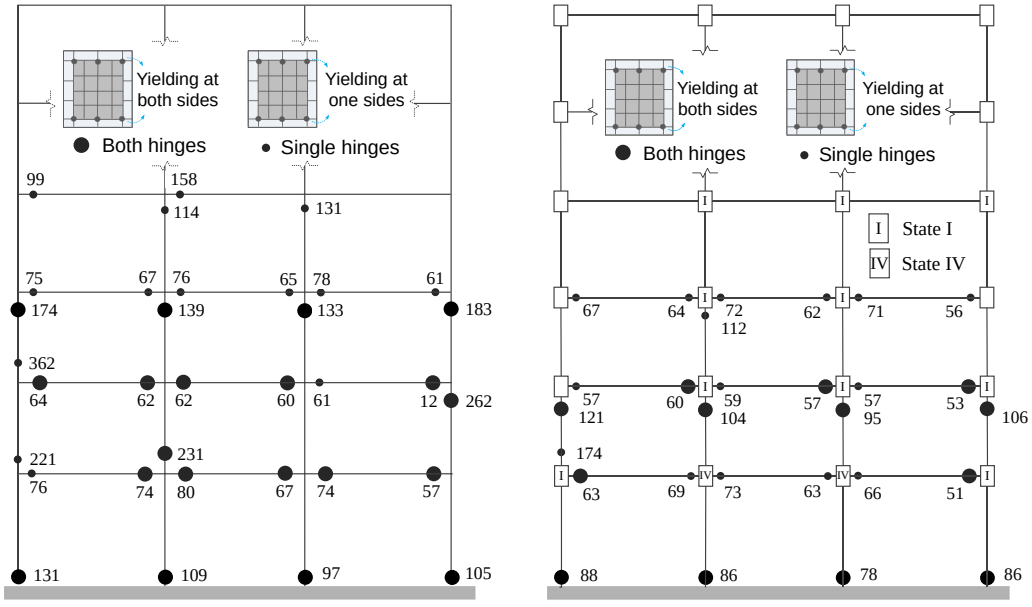


(a) Model without the proposed joint element (b) Model with the proposed joint element

**Fig. 19.** Structural failure modes of low-ductility structures.

predicted accurately, so joint element modelling is important and necessary for analysing existing RC frame buildings.

### 5.3. Failure mode analysis

For the newer design the maximum inter-storey drift was similar with or without the joint element, and the 3rd floor was the weak storey. However, for the low-ductility one the 2nd floor was the weaker storey with a larger drift than in the newer design. The distribution of the maximum inter-storey drifts for the woJoint and wJoint models was obviously different, as shown in Fig. 18.

In order to investigate the difference and to assess the seismic performance of the low-ductility structure, Fig. 19 shows the results of failure modes analyses for low-ductility structures with and without joint elements. The damage phases of the joint regions are divided into four states (Fig. 6), and the plastic hinges at the member ends are divided into two states representing rebar yielding at both sides (both hinges) or only one of them (single hinge) (Fig. 19). The load steps, the first yielding of the longitudinal steel, the distribution of plastic hinges at the member ends and final damage states of the joints are plotted in Fig. 19. Comparing Fig. 19(a) with (b) shows that for the model without joint elements, plastic hinges occur much later and the beams/columns suffer more severe damage than in the model with joint elements. If the joint has large shear deformation or joint failure appears, the ductility and the energy dissipation ability of the structure will be reduced, and collapses caused by joint failure will tend to happen. If the joint failure is prior to the members' failure, beams and columns would be protected to some extent, as shown in Fig. 19. This was also observed in multi-storey RC frame experiments with non-seismic detailing conducted by Yavari [32] in 2009. It can be seen that the seismic resistance of low-ductility structures performs weak with poor energy dissipation capacity, low collapse-resistance and brittle failure modes, and beam–column joints with low reinforcement ratios play an important role in these seismic capabilities. Just as what had been described in Dhakal's research [33] that joint modelling should be properly taken into account while dealing with the kinematics in the analysis of structures with low ductility.

## 6. Conclusion

A new beam–column joint element considering shear deformation and bar-slip behaviour has been proposed and evaluated against the quasi-static experimental results at the component level and the structure level. It was then applied to assess the seismic performance of the low-ductility structures built before the 1990s in China. On the basis of the results presented in this paper, the following conclusions can be drawn:

- The proposed joint element for simulating the response of joint sub-assembly has high accuracy for simulating initial stiffness, unloading stiffness and maximum column load, moderate accuracy for reloading stiffness, post yield stiffness, failure mode and pinching ratio.
- At the structural level, if joint shear deformation and beam rebar slippage are incorporated in the structural analysis by using the proposed joint element, the predicted results can be improved, especially the hysteretic performance, to be more consistent with experimental observations, so the proposed joint element is believed to be reliable and reasonable for simulating the response of RC structures.
- From the structural analysis, it can be found that joint failure tends to happen in low-ductility structures and it will reduce the ductility and the energy dissipation ability of the structure, even cause structural collapse. When joint failure happens prior to member failure, the local deformation would be concentrated on the joint panel and the surrounding beams and columns seem to be protected with little damage.
- Compared with the new designed structures, seismic performance of the low-ductility ones is undesirable, with poor energy dissipation capacity, weak collapse resistance and brittle failure modes. Joint modelling is necessary to be taken into account while dealing with the kinematics in the analysis of structures with low ductility.

## Acknowledgement

The authors gratefully acknowledge the financial support provided by China's National Natural Science Fund under grants 51261120376 and 91315301.

## Appendix A. Supplementary material

Supplementary data associated with this article can be found, in the online version, at http://dx.doi.org/10.1016/j.engstruct.2016.03.030.

## References

[1] Zhao B, Taucer F, Rossetto T. Field investigation on the performance of building structures during the 12 May 2008 Wenchuan earthquake in China. Eng Struct 2009;31(8):1707–23.
[2] Doğangün A. Performance of reinforced concrete buildings during the May 1, 2003 Bingöl Earthquake in Turkey. Eng Struct 2004;26(6):841–56.
[3] Ghobarah A, Saatcioglu M, Nistor I. The impact of the 26 December 2004 earthquake and tsunami on structures and infrastructure. Eng Struct 2006;28(2):312–26.
[4] Wu C, Chai J, Lin C J, et al. Reconnaissance report of 0512 China Wenchuan earthquake on schools, hospitals and residential buildings. In: Proc of 14th world conference on earthquake engineering, Beijing, China; 2008.
[5] Park R. A summary of results of simulated seismic load tests on reinforced concrete beam-column joints, beams and columns with substandard reinforcing details. J Earthquake Eng 2002;6(2):147–74.
[6] Hall JF. Northridge earthquake January 17, 1994. Preliminary reconnaissance report. Oakland (CA): Earthquake Engineering Research Institute; 1994.
[7] Ghobarah A, Biddah A. Dynamic analysis of reinforced concrete frames including joint shear deformation. Eng Struct 1999;21(11):971–87.
[8] El-Metwally SE, Chen WF. Moment-rotation modeling of reinforced concrete beam-column connections. ACI Struct J 1988;85(4):384–94.
[9] Alath S, Kunnath SK. Modeling inelastic shear deformation in RC beam-column joints. In: vol II. ASCE; 1995. p. 822–5.
[10] Uma SR, Prasad AM. Analytical modeling of RC beam-column connections under cyclic load. In: Proc of 11th world conference on earthquake engineering, Acapulco, Mexico; 1996.
[11] Fleury F, Reynouard JM, Merebet O. Multi-component model of reinforced concrete joints for cyclic loading. J Eng Mech 2000;126(8):804–11.
[12] Lowes LN, Altoontash A. Modeling reinforced-concrete beam-column joints subjected to cyclic loading. J Struct Eng 2003;129(12):1686–97.
[13] Mitra N, Lowes LN. Evaluation, calibration, and verification of a reinforced concrete beam–column joint model. J Struct Eng 2007;133(1):105–20.
[14] Anderson M, Lehman D, Stanton J. A cyclic shear stress–strain model for joints without transverse reinforcement. Eng Struct 2008;30(4):941–54.
[15] Birely AC, Lowes LN, Lehman DE. A model for the practical nonlinear analysis of reinforced-concrete frames including joint flexibility. Eng Struct 2012;34:455–65.
[16] Mitra N. An analytical study of reinforced concrete beam-column joint behavior under seismic loading. University of Washington; 2007.
[17] Ghannoum WM. Experimental and analytical dynamic collapse study of a reinforced concrete frame with light transverse reinforcement. Department of Civil and Environmental Engineering, University of California, Berkeley; 2007.
[18] Fu J, You Y, Bai S. Analysis on the force-transferring mechanism of the earthquake-resistant reinforced concrete frame joints. J Civ Archit Environ Eng 1996;18(2):43–52 [in Chinese].
[19] Vecchio FJ, Collins MP. The modified compression field theory for reinforced concrete elements subjected to shear. ACI Struct J 1986;83(2):219–31.
[20] Han F, Wang Z, Song M, et al. Strut-and-tie model method of reinforced concrete beam-column joint core. J Civ Archit Environ Eng 2010;32(1):61–5 [in Chinese].
[21] Ellingwood BR, Celik OC, Kinali K. Fragility assessment of building structural systems in mid-America. Earthquake Eng Struct Dynam 2007;36(13):1935–52.

[22] Fu J. Seismic behavior and design of joints in a reinforced concrete frame. Chongqing University; 2002 [in Chinese].
[23] Kim J, Lafave JM. Key influence parameters for the joint shear behaviour of reinforced concrete (RC) beam–column connections. Eng Struct 2007;29 (10):2523–39.
[24] ACI. Recommendations for design of beam-column connections in monolithic reinforced concrete structures. ACI 352-R02. ACI-ASCE Joint Committee 352, Farmington Hills, MI; 2002.
[25] GB 50011-2001. Code for seismic design of buildings. The construction ministry of PR China and National Bureau for Quality Supervision, Inspection and Quarantine; 2001.
[26] Mazzoni S, Mckenna F, Scott MH, et al. OpenSees users manual. PEER, University of California, Berkeley; 2004.
[27] Braga F, Gigliotti R, Laterza M. Analytical stress–strain relationship for concrete confined by steel stirrups and or FRP jackets. J Struct Eng ASCE 2006;132(9):1402–16.
[28] Anonymous. TJ11-78 code for seismic design of industrial and civil buildings. Beijing (China): China Architecture & Building Press; 1978 [in Chinese].
[29] Xu Y, Hu Q, Chen Y, et al. The experimental study of the behavior of a two-bay three-story RC frame under cyclic loading. J Build Struct 1986;2:1–16 [in Chinese].
[30] Lu X, Ye L, Pan P, et al. Pseudo-static collapse experiments and numerical prediction competition of a RC frame structure I: RC frame experiment. Build Struct 2012;42(11):19–22 [in Chinese].
[31] Zhang P, Ou J. Seismic performance analysis and evaluation for low-ductile RC frame structures. J Build Struct 2013;34(12):44–51 [in Chinese].
[32] Yavari S, Elwood KJ, Lin S, et al. Experimental study on dynamic behavior of multi-story reinforced concrete frames with non-seismic detailing. San Francisco: American Society of Civil Engineers; 2009.
[33] Dhakal RP, Pan T, Irawan P, et al. Experimental study on the dynamic response of gravity-designed reinforced concrete connections. Eng Struct 2005;27 (1):75–87.